Research Project

An Investigation of the Supersonic Blunt-Body Problem

Iliya Milman

Advisor: Dr. Michael Karp

Faculty of Aerospace Engineering

Technion - Israel Institute of Technology

November 2022

Abstract

This research studies the supersonic Blunt-Body Problem. A computational program is written which solves the inviscid steady-state flow around a blunt-body using an artificial time-marching technique. Flow fields around parabolic, cubic, and hyperbolic bodies are simulated and studied, these results are compared to previous research and their physical behaviour is assessed. Numerical experiments on the nature of the blunt-body problem are conducted. An oscillatory effect at the downstream boundary of the flow is observed and investigated.

1. Introduction

The blunt-body in supersonic flow is an important problem in aerodynamics because all high-speed vehicles have blunt noses to reduce aerodynamic heating. Such heating is a crucial design factor for most high-speed vehicles and its prediction requires accurate knowledge about the flow field around the body.

Historically, the inviscid supersonic blunt-body problem was appreciatively hard to solve because in the steady, subsonic regions of the flow the governing steady Euler equations are of elliptic nature, whereas in the supersonic regions they have hyperbolic nature. The situation changed in 1966 when Moretti and Abbett [1] published the first practical supersonic blunt-body solution. Their approach utilizes a time-marching finite-difference solution of the governing unsteady Euler equations. The unsteady Euler equations are hyperbolic with respect to time for both flow regions – subsonic and supersonic. Therefore, a time-marching approach allows a simultaneous solution of the flow in both regions.

The solution approach used in this study is the shock-fitting method. The shock wave is introduced in the solution as a boundary condition, and the Rankine-Hugoniot shock relations are used to relate the freestream to the flow behind the shock. The shock shape, therefore, is found as part of the solution. Using this approach, the whole flow field can be assumed to be isentropic, leading to a simplified energy equation.

Table of Contents

2. The Blunt-Body problem

Consider the steady flow over a blunt-body moving at supersonic speed. A schematic sketch of the problem is shown in Figure 1. The shock wave in front of this body is detached and curved. The incoming flow undergoes through variable shock angles, ranging from a normal shock wave at the nose tip and approaching a weak Mach wave away from the tip. The region between the shock and the body is called the shock layer, and it is a mixed subsonic–supersonic flow, with both regions divided by sonic lines. Behind the normal, and nearly normal, portions of the shock wave, the flow is subsonic, whereas behind the more oblique portion of the shock wave the flow is supersonic.

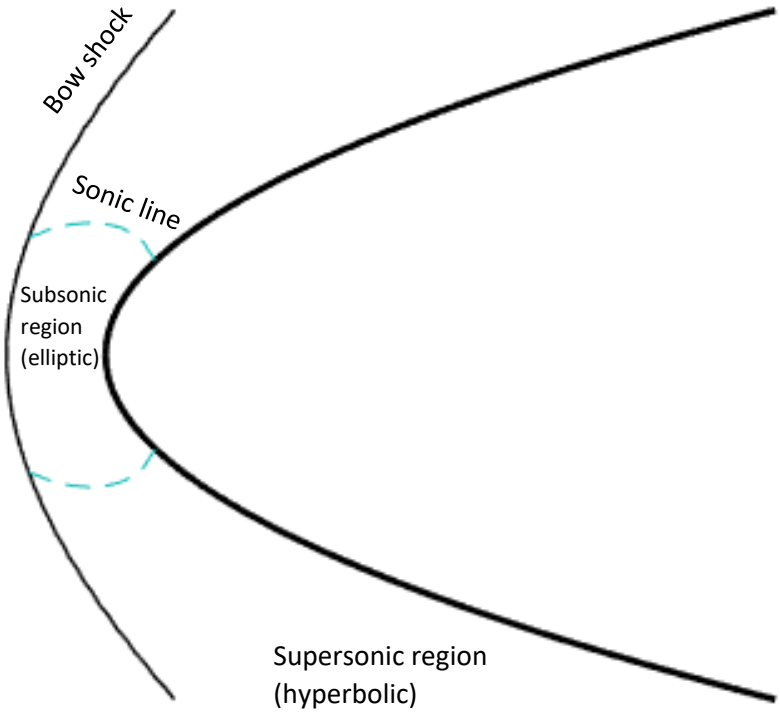

Figure 1: The blunt-body flow field

3. The Governing equations

The two-dimensional Euler equations describing the inviscid flow, are

x momentum

(1) $$\rho\left(\frac{\partial u}{\partial t}+u\frac{\partial u}{\partial x}+v\frac{\partial u}{\partial y}\right)=-\frac{\partial p}{\partial x},$$

y momentum

(2) $$\rho\left(\frac{\partial v}{\partial t}+u\frac{\partial v}{\partial x}+v\frac{\partial v}{\partial y}\right)=-\frac{\partial p}{\partial y},$$

continuity

(3) $$\frac{\partial \rho}{\partial t}+\frac{\partial(\rho u)}{\partial x}+\frac{\partial(\rho v)}{\partial y}+z\frac{\rho v}{y}=0,$$

where $z=0$ for the planar two-dimensional case and $z=1$ for the axisymmetric case.

The energy equation is replaced by the isentropic flow requirement, meaning it becomes an entropy equation.

(4) $$\frac{\partial}{\partial t}\left(\frac{p}{\rho^{\gamma}}\right)+u\frac{\partial}{\partial x}\left(\frac{p}{\rho^{\gamma}}\right)+v\frac{\partial}{\partial y}\left(\frac{p}{\rho^{\gamma}}\right)=0.$$

Coordinate Transformation

A simple computational grid is chosen where the physical variables x, y, t are transformed to the computational space variables ξ, Y, T such as

(5) $$\xi=\frac{x-b}{\delta}\quad Y=y\quad T=t,$$

where δ is the local shock-detachment distance, $\delta=s-b$, b is the body x coordinate and s is the shock x coordinate. The grids are shown below, the body is transformed to $\xi=0$, and the shock to $\xi=1$.

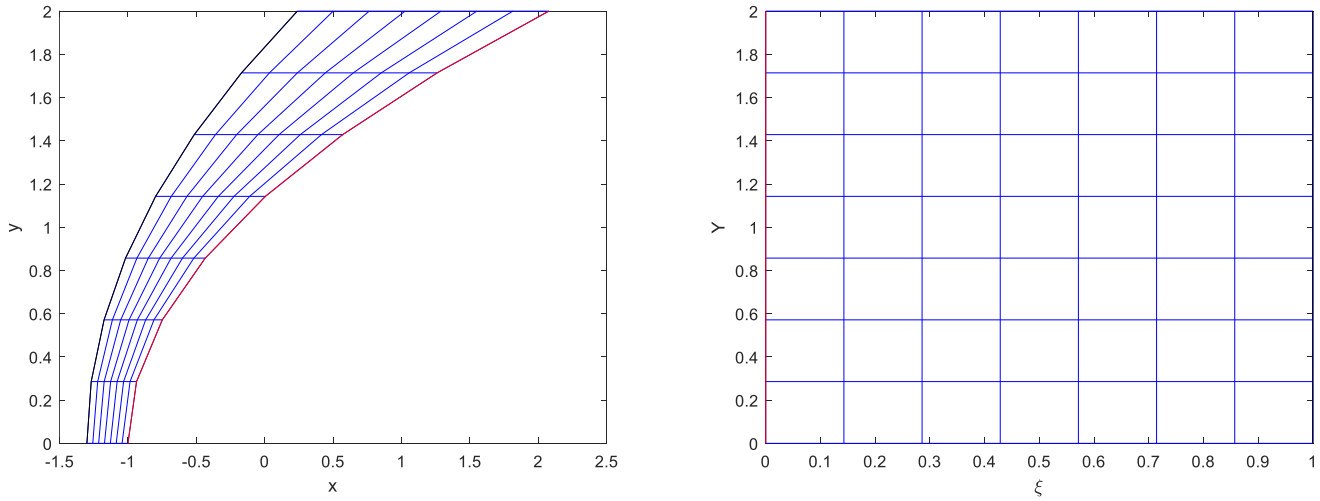

Figure 2: The physical and computational grids

For this transformation, any function $f(x, y, t)$ is transformed to

(6) $$\frac{\partial f}{\partial x} = \frac{1}{\delta}\frac{\partial f}{\partial \xi} \qquad \frac{\partial f}{\partial y} = \frac{\partial f}{\partial Y} + \frac{C}{\delta}\frac{\partial f}{\partial \xi} \qquad \frac{\partial f}{\partial t} = \frac{\partial f}{\partial T} - \frac{W\xi}{\delta}\frac{\partial f}{\partial \xi},$$

where

(7) $$C = (\xi - 1)\frac{db}{dy} - \xi cot\beta\ ,$$

(8) $$W = \frac{ds}{dt},$$

(9) $$\beta = \frac{\pi}{2} - \mathrm{atan}\frac{ds}{dy},$$

where W is the shock wave velocity and β is the shock angle.

For convenience, Moretti and Abbett's transformed variables will be used

(10) $$P = \ln p \qquad R = \ln \rho \qquad \psi = P - \gamma R \qquad B = \frac{u - W\xi + vC}{\delta},$$

Using all the relations described above the transformed Euler equations become

x momentum

(11) $$\frac{dv}{dT} = -\left[B\frac{\partial v}{\partial \xi} + v\frac{\partial v}{\partial Y} + \frac{PC}{\rho\delta}\frac{\partial P}{\partial \xi} + \frac{p}{\rho}\frac{\partial P}{\partial Y}\right],$$

y momentum

(12) $$\frac{\partial u}{dT} = -\left[B\frac{\partial u}{\partial \xi} + v\frac{\partial u}{\partial Y} + \frac{p}{\rho\delta}\frac{\partial P}{\partial \xi}\right],$$

Continuity

(13) $$\frac{\partial R}{\partial T} = -\left[B\frac{\partial R}{\partial \xi} + \frac{1}{\delta}\frac{\partial u}{\partial \xi} + \frac{C}{\delta}\frac{\partial v}{\partial \xi} + \frac{\partial v}{\partial Y} + v\frac{\partial R}{\partial Y} + z\frac{v}{Y}\right],$$

Energy

(14) $$\frac{\partial \psi}{\partial T} = -\left[B\frac{\partial \psi}{\partial \xi} + v\frac{\partial \psi}{\partial Y}\right].$$

4. The Numerical scheme

Choice of technique

Originally, Moretti and Abbett [1] used the Lax–Wendroff finite-difference technique. Later, MacCormack [2] developed a simpler explicit, predictor-corrector, finite-difference method which became very popular throughout the 1970s and 1980s. Because of its simplicity, it is used here.

MacCormack's Scheme

First, we calculate a predicted value of flow variable A from the first two terms in a Taylor's series

$$\bar{A}_{i,j}^{t+\Delta t} = A_{i,j}^{t} + \left(\frac{\partial A}{\partial t}\right)_{i,j}^{t} \Delta t, \tag{15}$$

where $\partial A/\partial t$ is calculated using forward differences for the spatial derivatives.

Next, as a corrector step, we calculate the value of the time derivative by inserting the predicted values using rearward differences for the spatial derivatives.

$$\left(\frac{\partial \bar{A}}{\partial t}\right)_{i,j}^{t+\Delta t}. \tag{16}$$

Then, by averaging those derivatives, we calculate the final corrected value of the variable.

$$A_{i,j}^{t+\Delta t} = \frac{1}{2}\left[\left(\frac{\partial A}{\partial t}\right)_{i,j}^{t} + \left(\frac{\partial \bar{A}}{\partial t}\right)_{i,j}^{t+\Delta t}\right]. \tag{17}$$

In the limit of large times, after enough steps, a steady state will be approached, at which $A_{i,j}^{t+\Delta t} \approx A_{i,j}^{t}$.

Regarding the numerical accuracy of this method, we are using first-order forward and rearward differences on the predictor and corrector steps, the combination of the two steps results in a second-order accurate technique.

For a time-marching approach, the value of Δt must be addressed. The finite-difference method used here is an explicit method, and therefore Δt is subject to a stability criterion.

The stability criterion is a version of the Courant–Friedrichs–Lewy (CFL) criterion, which governs the stability of explicit methods dealing with hyperbolic equations [6],

$$\Delta t < K\ \left[\min\left(\frac{\Delta x}{u+a}, \frac{\Delta y}{v+a}\right)\right], \tag{18}$$

where Δx and Δy the are the lengths between adjacent grid points in the x and y directions, and a is the local speed of sound, $a = \sqrt{\gamma RT}$.

The CFL criterion is derived based on an assumption of linearity. Therefore, for the nonlinear Euler equations a prefactor K is added, which is smaller than 1, in the current study a value of $K = 0.8$ is used.

4.1. Boundary conditions

For the shock wave boundary condition Moretti and Abbett [1] used a local, one-dimensional, unsteady method of characteristics obtained from the Rankine-Hugoniot relations for a moving shock. Similarly, for the body they used a local, unsteady, one-dimensional method of characteristics approach along the local body-normal direction. The approach used in the current study is simpler and reminiscent of the method provided by Anderson [3].

Shock wave

The quantities at the shock are calculated analytically using the Rankine-Hugoniot and oblique shock relations for the freestream values. In addition, the movement parameters of the shock must be calculated, mainly W and Δs - the shock movement distance. This is done by first calculating the flow properties at the shock boundary at time $t + \Delta t$, by employing the internal flow algorithm, using rearward differences in the predictor step. Using this method, the pressure at the next time step, $p(t + \Delta t)$, is calculated. In turn, from this pressure, and the known freestream condition, the static-pressure ratio, $p_2/p_1 = p(t + \Delta t)/p_\infty$, is obtained. Using this ratio and the wave angle, β, the shock wave is well-defined. As such, the Mach number of the flow upstream of the shock relative to the shock, M_1, is directly obtained from the shock relations. Then, the shock movement, W, is recovered by $W = a_\infty(M_\infty - M_1)$, where a_∞ is the freestream speed of sound.

With the wave velocity W at a given grid point the movement distance Δs in the x direction is calculated, where Δs is based on the average velocity between times t and $t + \Delta$t, that is

(19) $$\Delta s = \frac{1}{2}[W(t + \Delta \mathrm{t}) + W(t)]\Delta t.$$

Body

The boundary condition along the body is the inviscid no-penetration (slip) condition. First, the velocities at the boundary points are calculated using the internal flow algorithm. In this case, forward differences are utilized on both the predictor and corrector steps. Both velocity components u and v will be obtained at time $t + \Delta t$ at every grid point on the body. These components define the velocity vector V. To accomplish the desired boundary condition on the body, the vector V must be rotated to be tangential to the body, such that the velocity component normal to the surface, V_n, vanishes. After rotating V the remaining flow properties are treated by sending a local, one-dimensional, isentropic, expansion or compression wave away from the surface at the boundary point. The wave strength is calculated based on the pre-rotation value of V_n. If V_n is directed out of the surface, the finite wave should be an expansion wave, and if V_n is directed into the surface, the finite wave should be a compression wave.

The relations for pressure ratio and temperature ratio through an unsteady, isentropic, one-dimensional, finite wave are given in Chapter 7 of Anderson [5]. In our case, the equations for the finite wave are

(20) $$\frac{p_{new}}{p_{old}} = \left[1 \pm \frac{\gamma-1}{2}\left(\frac{V_n}{a_{old}}\right)^2\right]^{\frac{2\gamma}{\gamma-1}},$$

(21) $$\frac{T_{new}}{T_{old}} = \left[1 \pm \frac{\gamma-1}{2}\left(\frac{V_n}{a_{old}}\right)^2\right]^2,$$

where a_{old} is speed of sound from the previous iteration, V_n is taken positive and the plus sign corresponds to the expansion wave, while minus to the compression wave.

Downstream and centreline

The values for the points on the upper boundary are extrapolated from the inner values. As the downstream is taken far enough from the axis, such that the whole boundary is supersonic, the Euler equations there are hyperbolic. Because this condition is ensured, the extrapolation of the data should have no influence on the whole flow field. In the results sections, for faster computation, zeroth-order extrapolation is used.

For the centreline the usual symmetry condition is employed

(22) $$p_{j+1} = p_{j-1} \; ; \; T_{j+1} = T_{j-1} \; ; \rho_{j+1} = \rho_{j-1} \; ; v_{j+1} = -v_{j-1}.$$

This symmetry condition is sufficient to form the forward and rearward differences at grid points along the centreline, thus allowing the use of the usual internal flow algorithm to calculate properties along the centreline.

The initial flow field

The computation is sensitive to the assumed initial conditions, and the initial flow field influences on the “go” or “no-go” nature of the blunt-body computer program. The assumed initial flow field is obtained by the logic presented in Anderson and Albacete [4].

1. A parabola as initial shock wave shape multiplied by some factor less the unity.
2. Modified Newtonian pressure distribution along the body surface.
3. Isentropic expansion along the body streamline.
4. Linear interpolation between the shock and the body.
5. A shock detachment distance assumed by trial and error.

5. Results

This chapter presents the flow fields around the following blunt-bodies at M_∞ of 4 and 8:

I. Parabolic cylinder, with the cross-section

(23) $$b = ay^2 - 1,$$

where $a = 0.769$.

II. Hyperbolic cylinder, with the cross-section

(24) $$b = \sqrt{\left(\frac{y}{a}\right)^{0.5} + 1} - 2,$$

where $a = 0.769$.

III. Cubic cylinder, with the cross-section

(25) $$b = a_2 y^3 - 1,$$

where $a_2 = 0.427$.

IV. Paraboloid of revolution, with the cross-section

(26) $$b = ar^2 - 1,$$

where $a = 0.769$.

A drawing of the blunt-bodies is given in the following figure

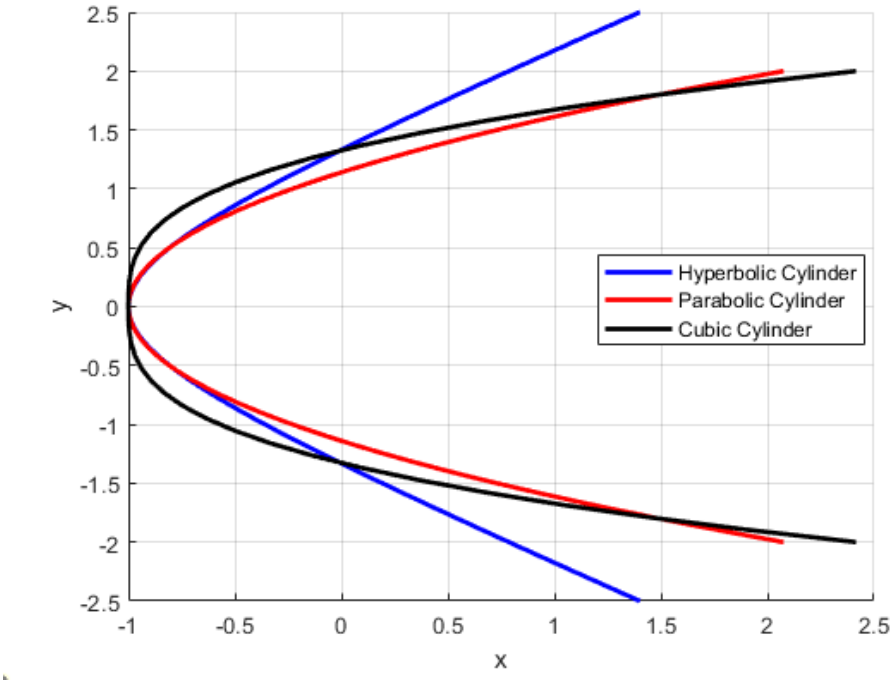

Figure 3: The blunt-body shapes

The number of grid points for each case is presented in the table below

$M_\infty = 4$	ξ points	y points
Cubic cylinder	8	30
Hyperbolic cylinder	12	30
Parabolic cylinder	8	30
Paraboloid	8	30
$M_\infty = 8$	–	-
Cubic cylinder	15	30
Hyperbolic cylinder	12	30
Parabolic cylinder	10	30

For the axisymmetric body, the paraboloid, only results for $M_\infty = 4$ are shown, due to an oscillatory effect at the downstream boundary which allows simulation of small axisymmetric flow fields only. The influence of this effect can be seen in all the two-dimensional results and will be discussed in detail later.

In addition, for all the results

- A calorically perfect gas with $\gamma = 1.4$.
- For fast computation, a zero-order extrapolation is used at the downstream

For the surface pressure distribution, the modified Newtonian pressure distribution is given for comparison. The modified Newtonian formula is

(27) $$C_p = C_{pmax} \sin^2 \theta,$$

where θ is the local body angle and C_{pmax} is the maximal pressure coefficient, evaluated for the stagnation pressure, $p_{0,2}$, after a normal shock at the axis

(28) $$C_{pmax} = \frac{p_{0,2} - p_\infty}{\frac{1}{2}\rho_\infty U_\infty^2}.$$

In addition, the results for the entropy, S, with respect to its freestream value, S_∞, normalized by the air specific gas constant, R, are shown

(29) $$\frac{S - S_\infty}{R} = \frac{1}{\gamma - 1}\left(\ln\frac{p}{p_\infty} - \gamma \ln\frac{\rho}{\rho_\infty}\right) = \frac{1}{\gamma - 1}\left(\psi - \psi_\infty\right).$$

5.1. Shock wave location

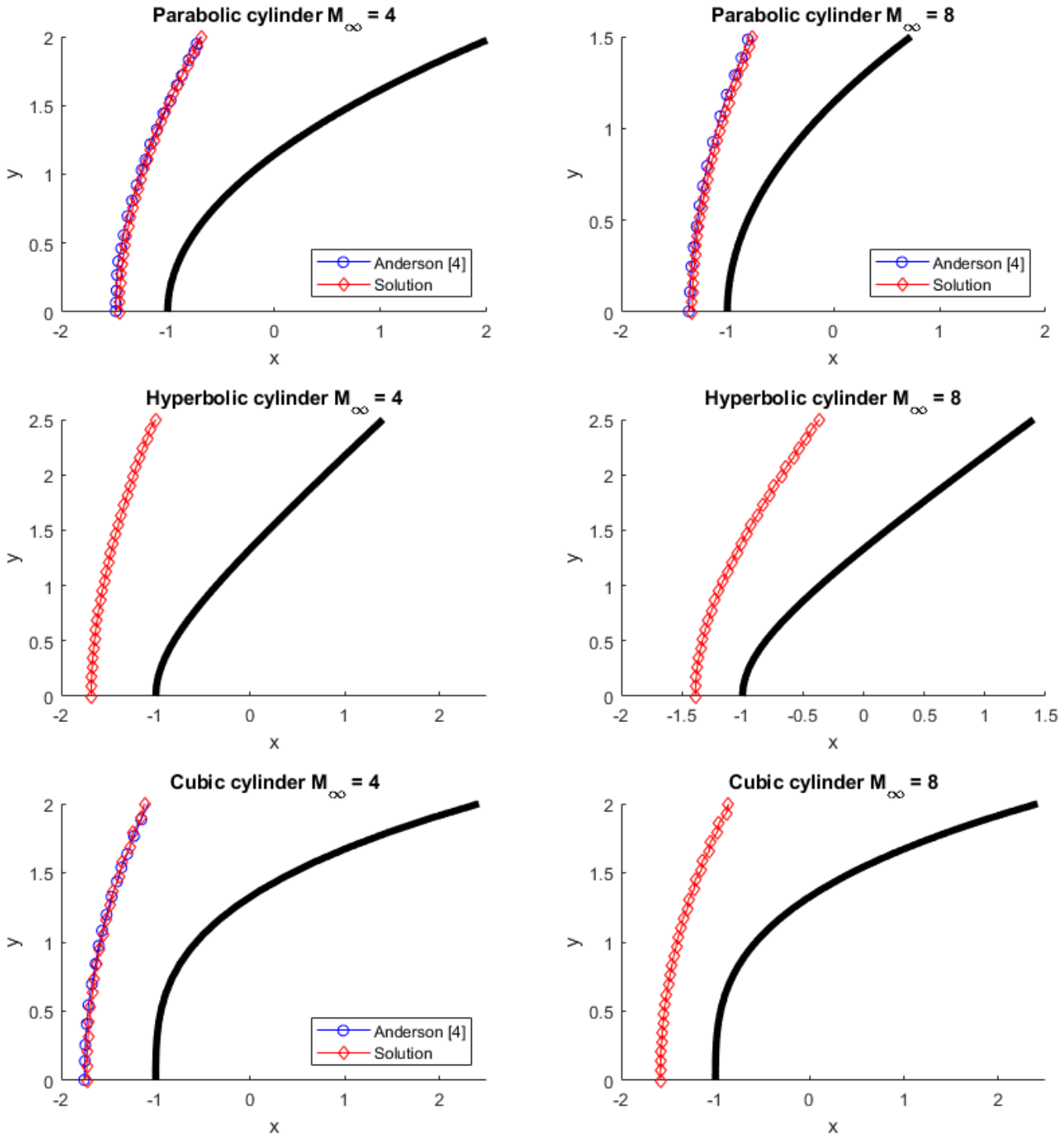

Figure 4: Shock wave location for various blunt-bodies

The steady state shock wave location is presented and compared to Anderson [4], good agreement is seen. Also, it can be observed that as M_∞ increases, as expected, the shock wave moves closer to the body.

5.2. Sonic line Location

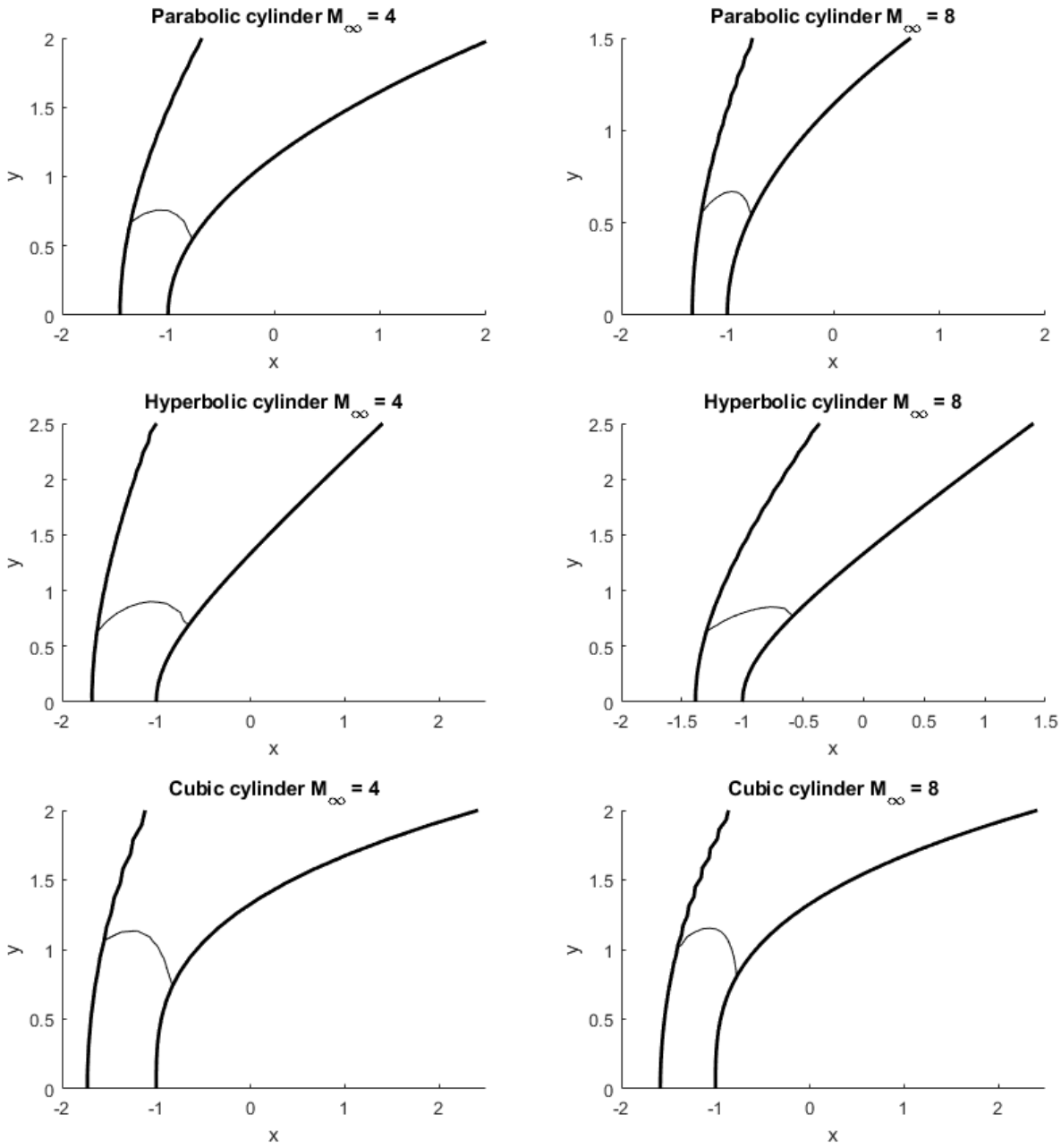

Figure 5: Sonic line location for various blunt-bodies

In figure 5, the sonic lines shape and location are presented, and standard physical behaviour for blunt-body flows is seen. For all the blunt-bodies, as M_∞ increases the body sonic point moves closer to the centreline, while the shock sonic point moves towards the point with the highest curvature. This point is closer to the centreline for the hyperbolic and parabolic cylinders, and away from the centreline for the cubic cylinder.

5.3. Entropy field

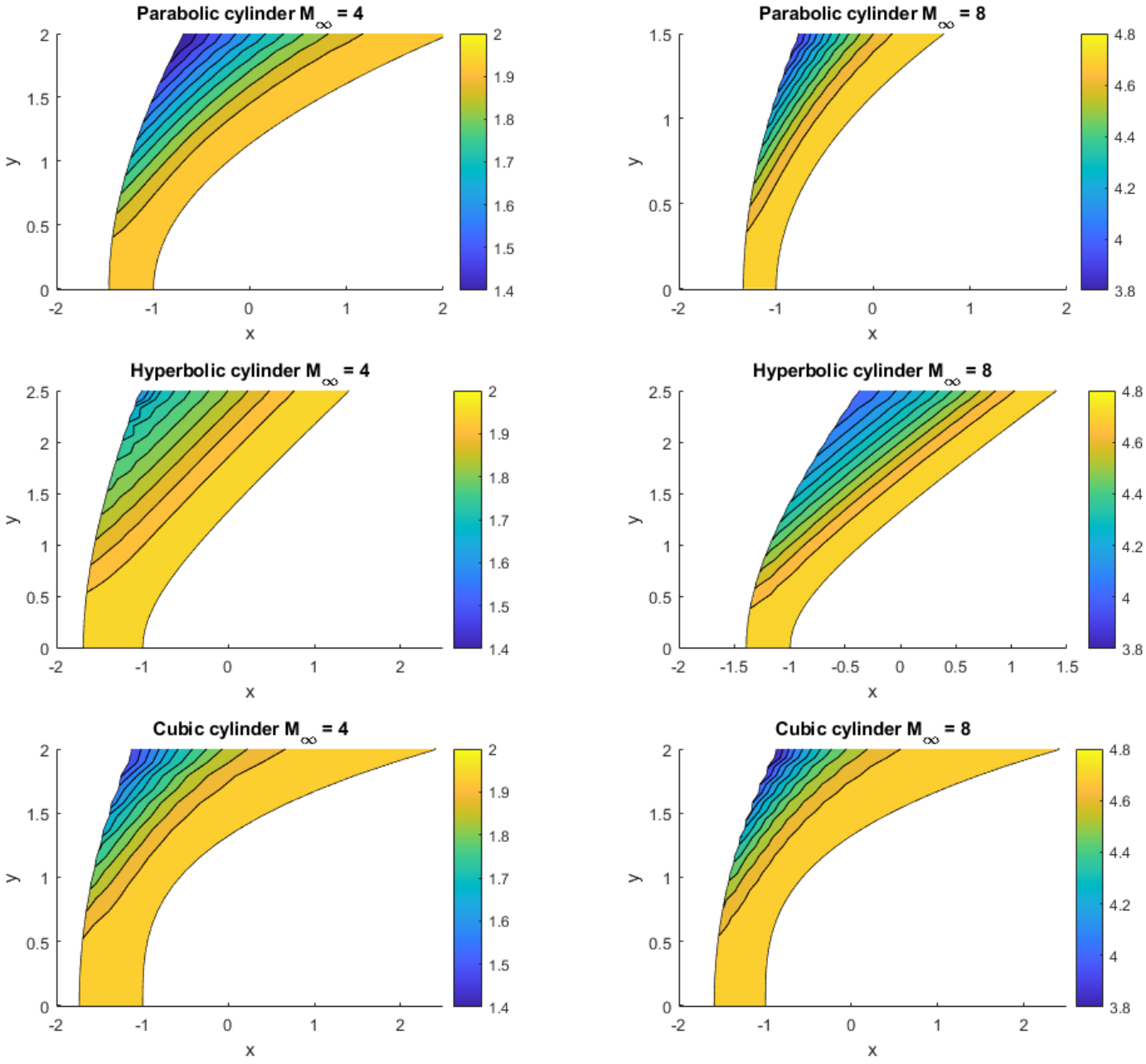

Figure 6: Entropy field for various blunt-bodies

Figure 6 shows the non-dimensional entropy field, $(S - S_\infty)/R$, as detailed in equation (29). Because the flow is isentropic, the constant entropy lines are identical to the streamlines. Further away from the body, many constant entropy lines are seen, which means there is a high gradient of entropy far from the body. Close to the body, a thick high-entropy layer appears, this type of entropy layer is typical for two-dimensional blunt-body problems.

5.4. Pressure field

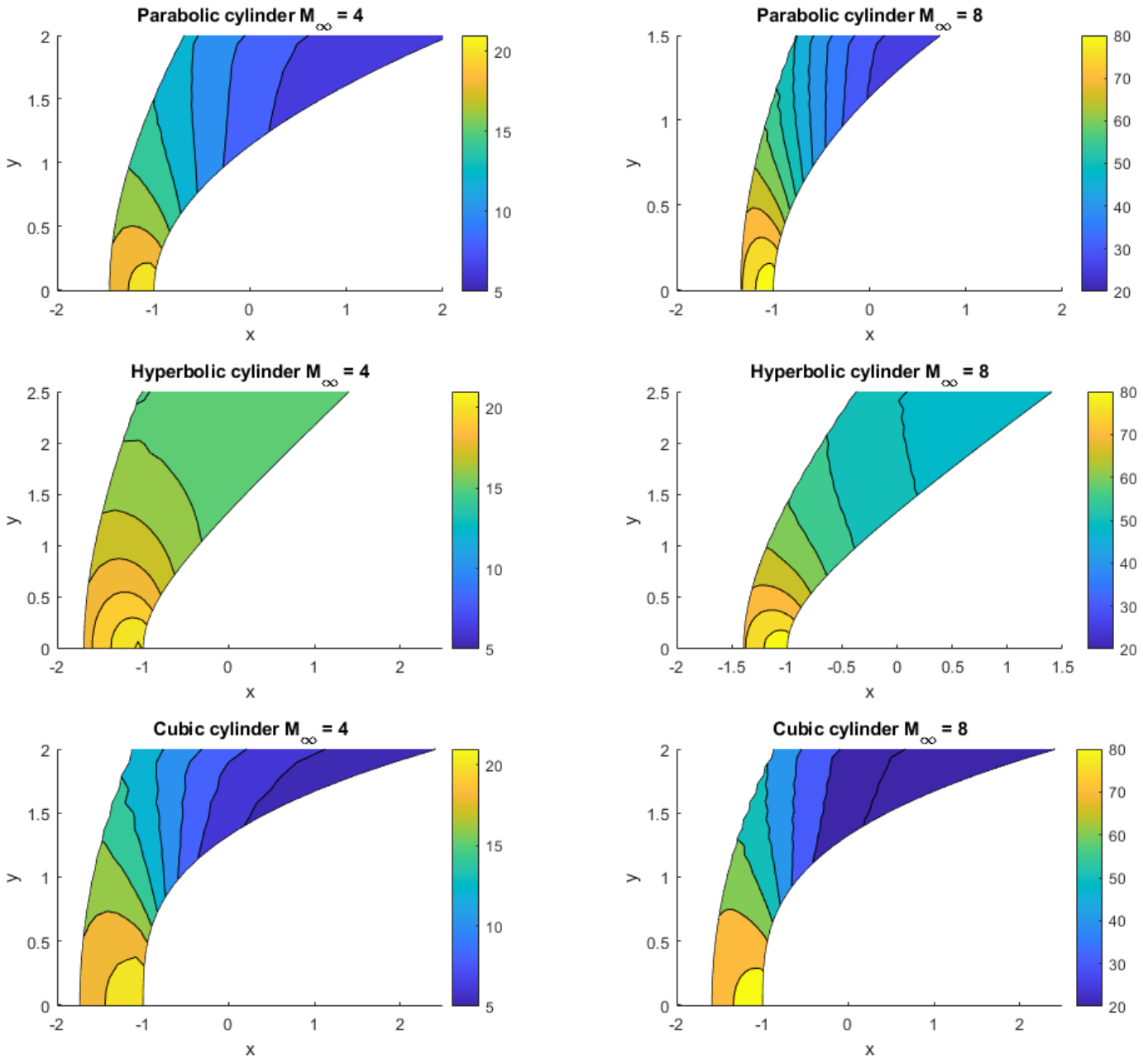

Figure 7: Pressure field for various blunt-bodies

In figure 7, the static pressure ratio, p/p_∞, distribution is presented. Behind the normal part of the shock, the static pressure ratio p/p_∞ is 18.5 and 74.5 for $M_\infty = 4$ and $M_\infty = 8$, respectively. At the weak part of the shock downstream, the average static pressure ratio is 14 and 50 for $M_\infty = 4$ and $M_\infty = 8$, respectively. In addition, the oscillatory effect can be seen in the upper part of the flow field downstream.

5.5. Velocity field

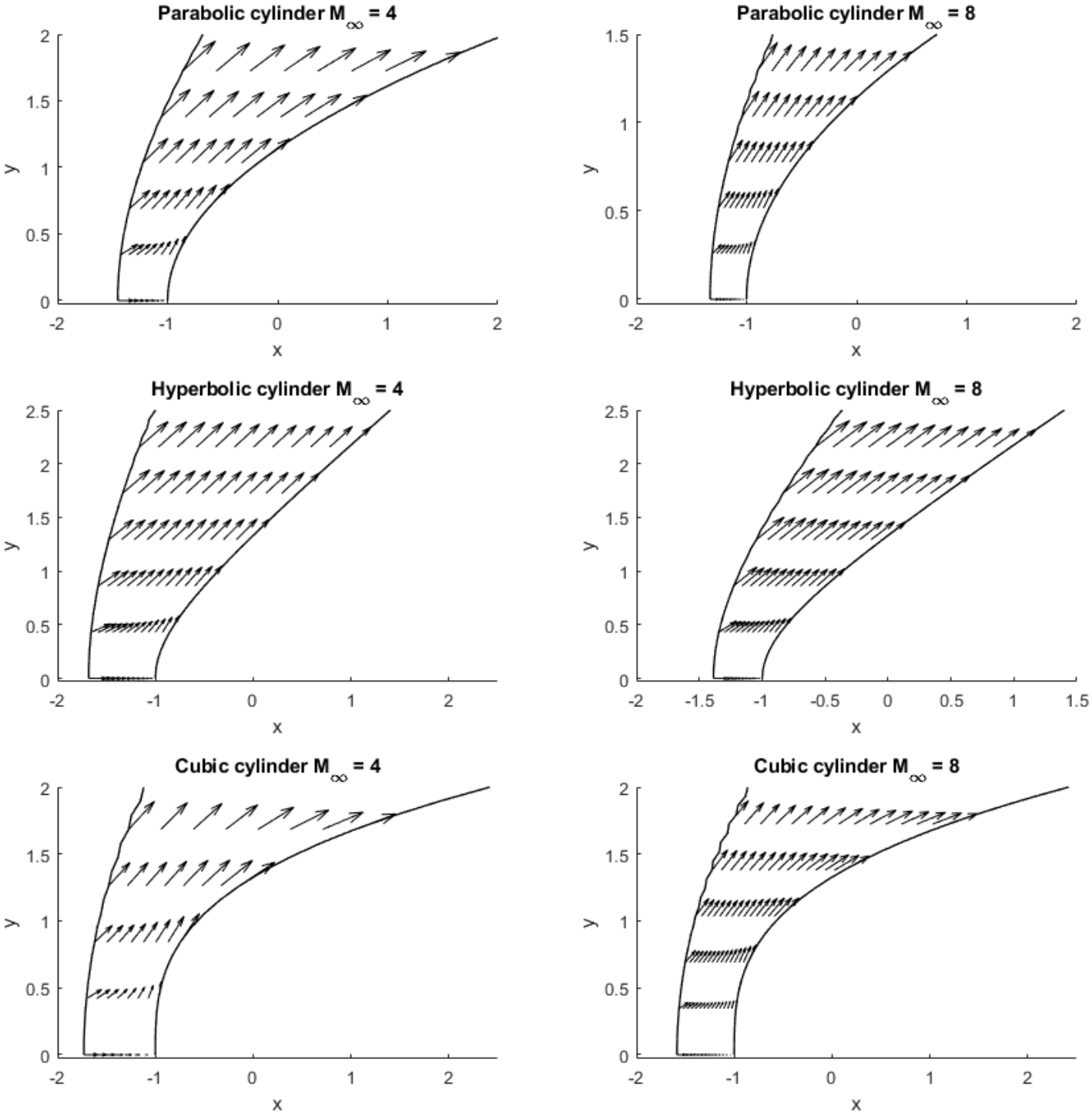

Figure 8: Velocity vectors for various blunt-bodies

Figure 8 shows the velocity vectors. The velocity vectors closely follow the constant entropy lines, confirming entropy is conserved along streamlines. In addition, close to the body, slip flow is happening, and an acceleration of the flow is also observed.

5.6. Surface pressure distribution

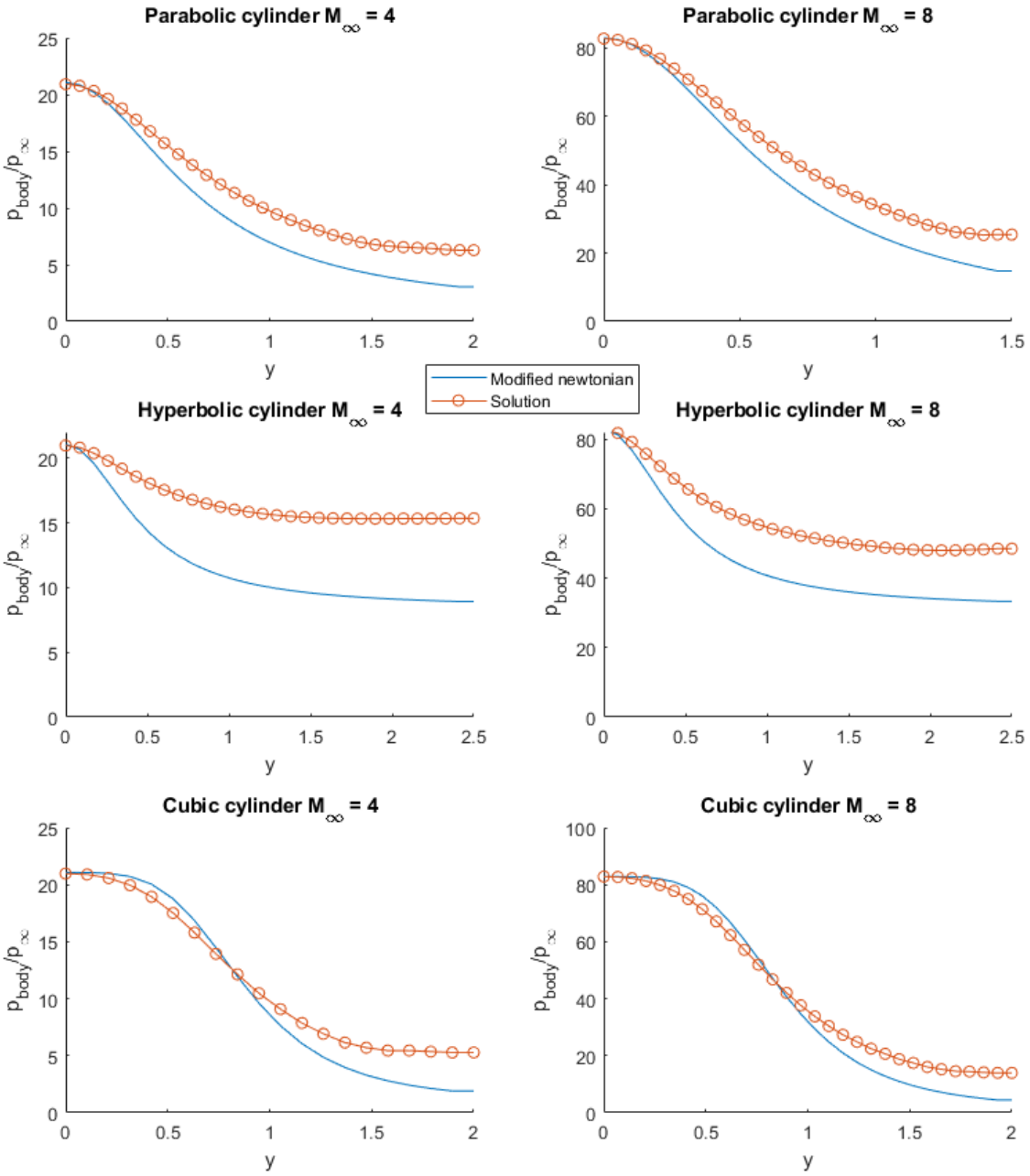

Figure 9: Surface pressure distribution for various blunt-bodies

Figure 9 shows the surface pressure distributions, normalized with respect to freestream pressure p_{body}/p_{∞}. These results are compared with the modified Newtonian formula, and two anticipated results can be seen. Namely, that the modified Newtonian distribution underestimates the actual pressure distribution for two-dimensional blunt-bodies, and the resulting distribution is closer to the modified Newtonian at $M_{\infty} = 8$ than at $M_{\infty} = 4$. This is expected since the Newtonian theory was derived in the limit $M_{\infty} \to \infty$.

5.7. Centreline wave velocity and Stagnation pressure history

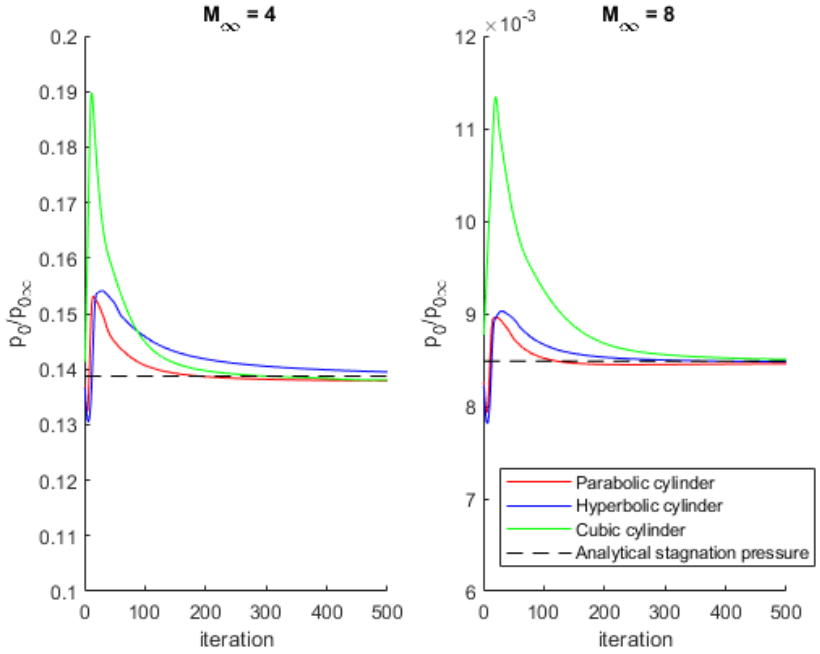

Figure 10: Stagnation pressure history for various blunt-bodies

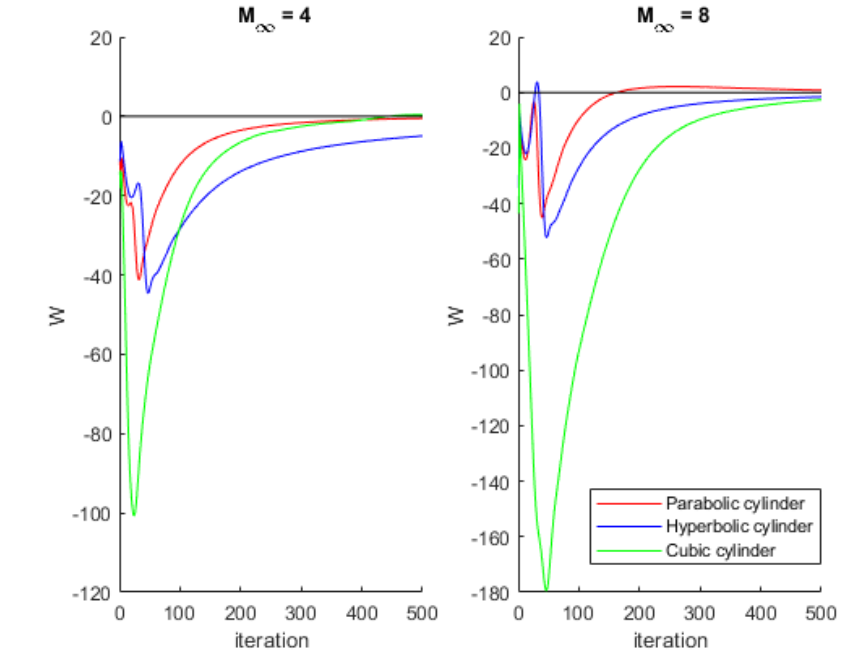

Figure 11: Centreline shock wave velocity history for various blunt-bodies

Figures 10 and 11 show the convergence paths for all blunt-bodies studied above. Figure 10 shows the time variation of stagnation-point pressure, and figure 11 presents the transient behaviour of the centreline shock wave velocity. In all cases, the assumed initial values are similar. Some points are noted from the above figures: the biggest variations occur at early times. In addition, the cubic cylinder has the largest variations, caused probably due to its initial shock wave shape (parabola) being far from its final shock shape, compared to the other two shapes.

5.8. Axisymmetric case

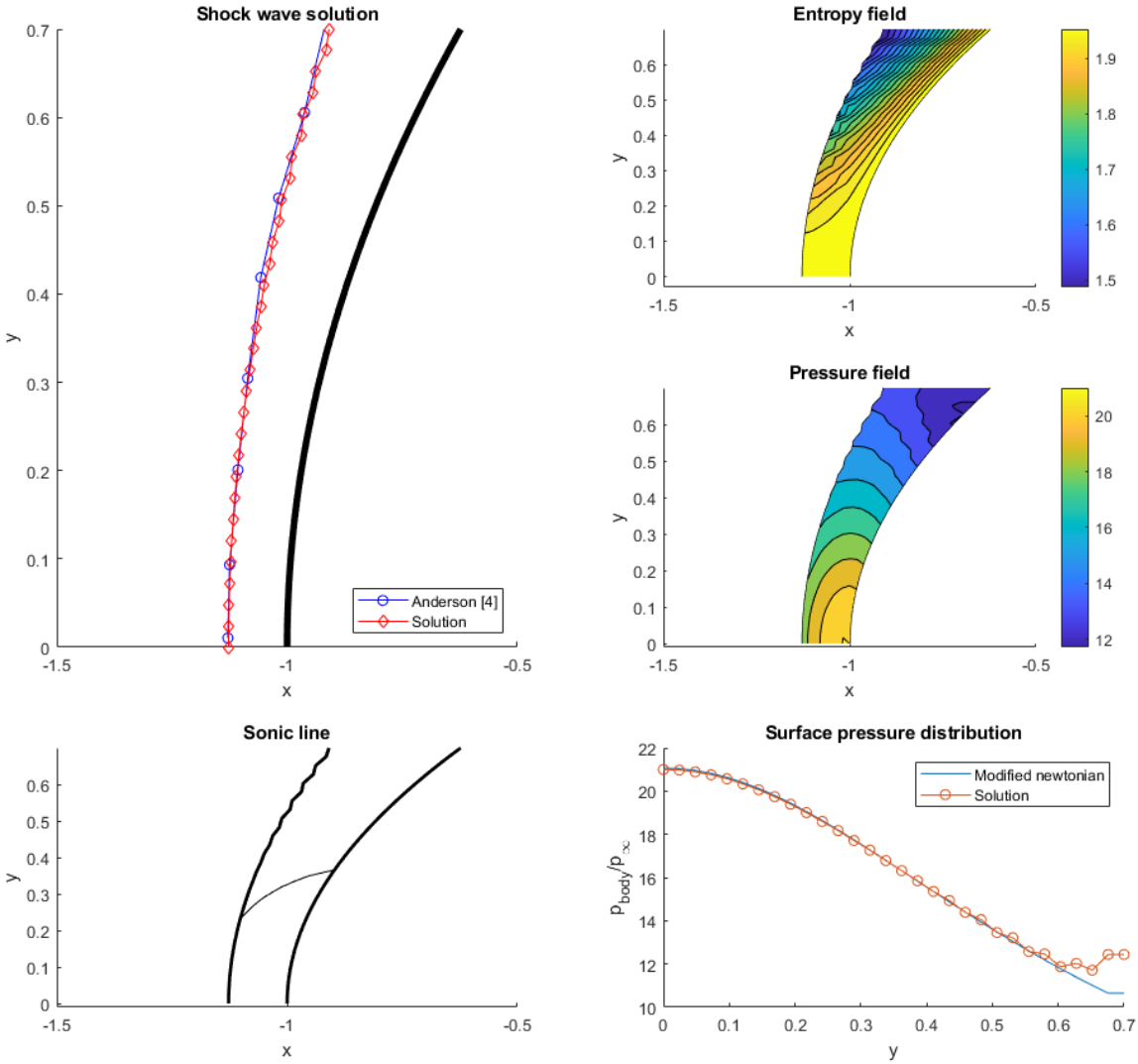

Figure 12: Results for axisymmetric paraboloid, $M_\infty = 4$

When examining the axisymmetric results, the oscillatory effect has a significant influence on the axisymmetric flow field, which destabilizes the computer program. This effect accelerates some parts of the shock faster than others, resulting in a negative shock wave angle β which in turn collapses the program. In addition, a major surface pressure instability in the downstream boundary can be observed and the solution in this area can be assumed to be invalid. Although results for a flow field with the same size as the one used in the two-dimensional case could not be obtained, some parts of the flow field could still be simulated, provided y_{max} is sufficiently small. In figure 12 good agreement of the shock wave location can be seen between the solution and the reference. Regarding the entropy field, for the axisymmetric results, in contrary to the two-dimensional results, no thick entropy layer is present, and the constant entropy lines converge towards the body, which is a known phenomenon for axisymmetric fields. In addition, very good agreement between the solution and the modified Newtonian theory is observed, even away from the centreline, which is typical for axisymmetric flow fields.

6. Numerical experiments on the sensitivity of the blunt-body solution to selected parameters

In addition to the above results, numerical experiments were performed to investigate the effect of initial conditions, shock shape, and boundary conditions on the time-dependent blunt-body solutions. The experiments indicate that such factors have a definite influence on the blunt-body computer program.

Effect of the initial shock shape

The computer program was able to converge using a shape similar to the shape of the body. However, the initial shock shape has an influence on the range of the initial shock-detachment distance guess that leads to a converged solution. In most cases, it was found that a parabolic shock shape with an incline similar to the body multiplied by a prefactor smaller than unity could sustain the farthest initial shock-detachment distance. For example, for the cubic cylinder given by

(30) $$b = ay^3 - 1,$$

the following shock was assumed

(31) $$s = factor \cdot ay^2 - 1.$$

The factor also has an influence on the convergence of the computer program and is chosen by trial and error. For the various blunt-body shapes used in the study, a factor of 0.2 was used.

Effect of shock-detachment distance

The initial shock-detachment distance, together with the shock shape, have a great influence on the convergence of the computer program. For example, for the case of a two-dimensional parabolic body and initial parabolic shock shape multiplied by a factor of 0.2 at $M_\infty = 4$ the program converged successfully for $0.3 < \delta < 1.2$.

Effect of extrapolation order on the upper boundary

The values on the downstream boundary are extrapolated from the internal grid points. It is ensured that the downstream boundary is far enough so that the flow is supersonic when approaching the boundary. That is because extrapolation in any order is a properly posed supersonic boundary condition. Consequently, the upper boundary values do not exactly satisfy the Euler equations, and therefore the results for certain portions of the flow field are inaccurate. Our findings suggest that the extrapolation influences substantial parts of the flow and not just the boundary.

The extrapolation was suspected as the reason for the appearance of oscillations near the downstream. To study this effect, the following numerical experiments with the downstream boundary condition were conducted

- First-order linear extrapolation.
- Zeroth-order extrapolation.
- Using the internal algorithm with one-sided finite-differences.

A result of these experiments for a parabolic cylinder at $M_\infty = 4$ is shown in Figure 13 below.

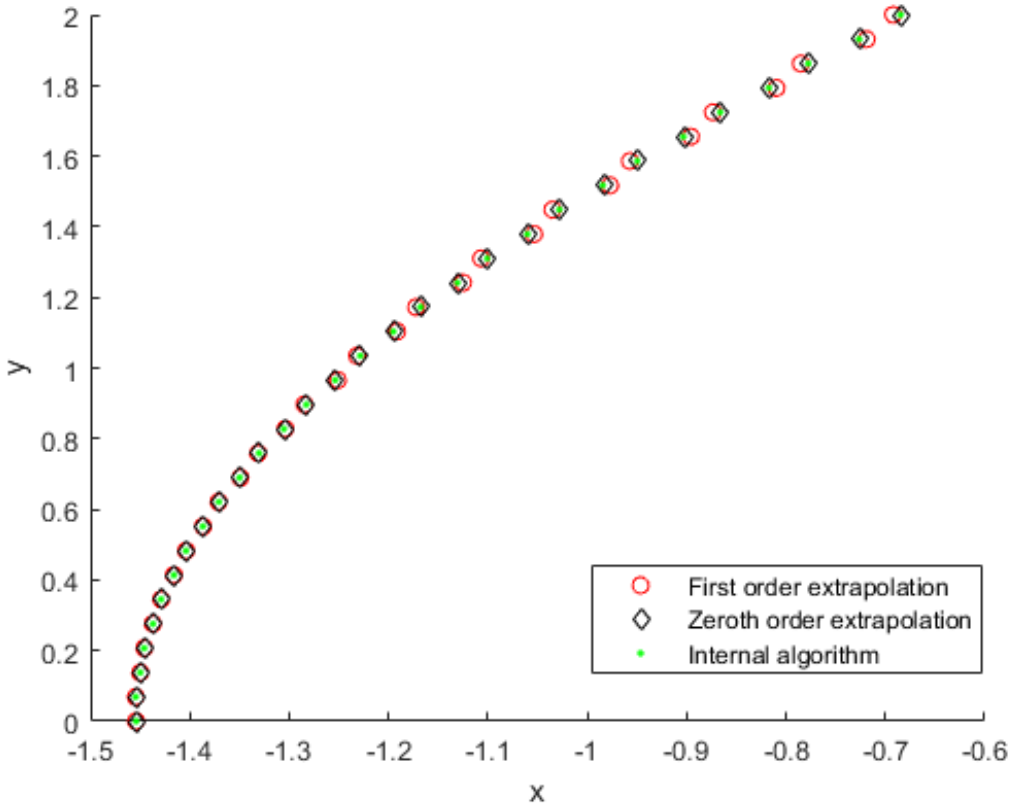

Figure 13: shock wave solution for parabolic cylinder at $M_\infty = 4$ using various downstream boundary condition treatments

No significant effect on the oscillation is observed, and it seems that the extrapolation is not fully or not at all responsible for this effect.

Effects of the computational grid length in the y direction

The computational grid length in the y direction, y_{max}, has a strong influence on the oscillatory effect downstream. In particular, choosing a lower y_{max} seems to reduce this effect, and provide smoother results. Furthermore, the type of body and the freestream velocity influences the oscillations. For the hyperbolic body, a flow field larger than the one for the cubic cylinder is successfully simulated. In addition, for the axisymmetric case, very low y_{max} had to be chosen to get a converged solution.

7. Conclusions and future research

This research investigates the supersonic blunt-body problem. A computational program is written to numerically solve the blunt-body problem, and a study of both the computer program and the solution is performed. The solution is compared to previous research, and good agreement is observed. In addition, the flow field is studied and known physical behaviour is recovered. In the case of the program, an unwanted oscillatory effect at the downstream boundary of the flow is present. Numerical experiments to study this effect and the influence of the initial flow field on the computer program are conducted.

The computer program is found to be sensitive to the initial conditions. A combination of several parameters, mainly the initial shock shape and shock detachment distance, determines the “go” or “no go” nature of the program.

Regarding the downstream oscillatory effect, it is found that the size of the grid along the y direction has the main influence on this effect. Choosing a large value for y_{max} causes the solution to have stronger oscillations, and when the value of y_{max} increases beyond a certain limit, the computer program collapses. The critical value of y_{max} is influenced by the body type, the freestream velocity, and whether it is a two-dimensional or an axisymmetric case. Owing to this effect, only small axisymmetric flow fields were able to be simulated.

Typical behaviour for the blunt-body flow field is observed. At higher free stream velocities, the bow shock moves closer to the body and the sonic line moves closer to the centreline. For the two-dimensional field, a thick entropy layer is formed, while for the axisymmetric field the entropy lines converge towards the body. In addition, the modified Newtonian formula underestimates the body pressure distribution for the two-dimensional field and predicts good values for the axisymmetric case, as expected.

In the future, the cause and solution of the oscillatory effect should be addressed. With this effect gone, larger axisymmetric flow fields could be simulated and analysed. In addition, studies of the propagation of weak shock disturbances in the flow field could be conducted. Another possible improvement is providing a method to get an initial shock detachment distance and shock shape without the need for trial and error.

References

[1] Moretti, G., and Abbett, M., “A Time-Dependent Computational Method for Blunt-Body Flows”, AIAA Journal, Vol. 4, No. 12, 1966, pp. 2136–2141.

[2] MacCormack, R. W., “The Effect of Viscosity in Hypervelocity Impact Cratering”, AIAA Paper 69-354, Jan. 1969.

[3] Anderson, J. D., Jr., “Hypersonic and High Temperature Gas Dynamics”, 2nd ed. 2006.

[4] Anderson, J. D., Jr., and Albacete, L. M., “On Hypersonic Blunt-Body Flow Fields Obtained with a Time-Dependent Technique”, Naval Ordnance Lab., NOLTR 68–129, White Oak, MD, Aug. 1968.

[5] Anderson, J. D., Jr., “Modern Compressible Flow: with Historical Perspective”, 3rd ed. McGraw–Hill, New York, 2003.

[6] Courant, R., Friedrichs, K. O., and Lewy, H., “Uber die Differenzengleichungen der Mathematischen Physik”, Math. Ann., Vol. 100, 1928, p. 32.